Progress in Physics of Applied Materials 2 (2022) 63-69

Semnan University

Progress in Physics of Applied Materials

journal homepage: https://ppam.semnan.ac.ir/

Solid state and hydrothermal synthesis, characterization and optical properties of $Yb_2V_2O_7$

Samira Hadilou, Mahdi Behzad*, Shahin Khademinia*

Department of Inorganic Chemistry, Faculty of Chemistry, Semnan University, Semnan, Iran

ARTICLE INFO

Article history:
Received: 22 December2021
Revised: 15 July 2022
Accepted: 18 October 2022

Keywords:
$Yb_2V_2O_7$
Hydrothermal Method
Nanomaterial
Solid State Method
Cyclic Voltammetry

ABSTRACT

$Yb_2V_2O_7$ nano-powders were synthesized via solid state and hydrothermal reactions using Yb_2O_3 and Na_2VO_4 at stoichiometric 1:1 Yb:V molar ratio as raw materials for the first time. The synthesized materials were characterized by powder X-ray diffraction (PXRD) technique. Structural analysis was performed by *FullProf* program employing profile matching with constant scale factors. The results showed that the patterns had a main $Yb_2V_2O_7$ structure with a space group of $Fd\bar{3}m$. Besides, the data revealed that the reaction conditions affected the physical property and crystal phase growth of the obtained materials. FESEM images showed that the synthesized $Yb_2V_2O_7$ particles had mono-shaped sphere morphologies. Ultraviolet–visible spectroscopy (UV-Vis) analysis showed that the nanostructured $Yb_2V_2O_7$ powders possessed strong light absorption properties in the ultraviolet-visible light region. The direct optical band gaps were 3.90, 4.10, 4.15, and 4.35 eV for S_1, S_2, S_3, and S_4, respectively. Electrochemical property of $Yb_2V_2O_7$ nanoparticle was studied by cyclic voltammetry (CV) technique in NaOH electrolyte medium.

1. Introduction

Oxides and fluorites with general formula $A_2B_2O_7$ (where A is a medium – large cation and B is an octahedrally coordinated, high – charge cation) have been studied extensively. Pyrochlore materials with general formula $A_2B_2O_7$ relate to the fluorite structure and the nature of this relationship is discussed in the crystallography of this compounds [1]. There are few compounds that have simultaneously ferromagnetic and semiconductor properties. One of the compounds is $Yb_2V_2O_7$. Rare earth ortho vanadates are important class of inorganic functional materials studied extensively for their structural and chemical properties. $Yb_2V_2O_7$ has pyrochlore type structure. According to reported researches conducted on $Yb_2V_2O_7$ materials, it has been found that $Yb_2V_2O_7$ crystallizes in cubic crystal structure with space group $Fd3^{-}m$. These compounds have unique physical properties such as catalysis [2-5], electronic [6], magnetic properties [7, 8], optical properties [9], and are used in solid oxide fuel cells (SOFC) [10]. Also, the compound has the ferromagnetic property with the highest value of TC, so it can be ideal option for use on different devices from computer to high temperature sensors. Some methods have been reported for the synthesis of $Yb_2V_2O_7$ nanomaterials such as solid state using VO_2 and Yb_2O_3 [11], floating – zone [12], and heating $REVO_4$ [13]. There are many reports about magnetic data found for $Yb_2V_2O_7$ nanomaterials [14] and $Yb_2V_2O_7$ via this method, including floating – zone method [15, 16], flux growth method [17-19], hydrothermal method [20], liquid – phase method [21, 22], melt- mode method [23], precipitation method [24]. The samples were pressed up to 25 GPa for 2 h and then released to ambient conditions [25] and solid-phase synthesis method was applied [26]. In the present work, hydrothermal and solid state method have been successfully used for the synthesis of $Yb_2V_2O_7$ nanostructure using Yb_2O_3 and Na_3VO_4 as raw materials. $Yb_2V_2O_7$ was synthesized for the first time via hydrothermal route. There is no report on the synthesis of the $Yb_2V_2O_7$ nanostructure by this method. Crystalline phase growth of the synthesized materials in different conditions is investigated using Rietveld analysis. Physical properties of the synthesized nanomaterials were studied using field emission scanning electron microscope (FESEM), ultraviolet visible (UV-Vis) spectroscopy, Brunauer Emmett teller (BET), and Barrett Joyner Halen (BJH) methods. titanium ions.

2. Experimental

* Corresponding author. Tel.: +98-912-2312970
E-mail address: mbehzad@semnan.ac.ir , shahinkhademinia@alum.semnan.ac.ir

DOI: 10.22075/ppam.2022.25660.1018

2.1. Materials and instruments

All chemicals including Yb_2O_3, Na_3VO_4, and NaOH were of analytical grade and obtained from commercial sources (Merck Company) and used without further purifications. Phase identifications were performed on a powder X-ray diffractometer D5000 (Siemens AG, Munich, Germany) using CuK_α radiation. The Rietveld analysis was performed by *FullProf* software. The morphology of the obtained materials was examined with a field emission scanning electron microscope (Hitachi FE-SEM model S-4160). The surface area, pore volume and average particles size were calculated using the Brunauer-Emmett-Teller (BET) equation. Pore size distributions, pore volume and pore surface area were calculated by the Barrett-Joyner-Halenda (BJH) method. The data were collected on a Beckman Coulter SA3100 Surface Area Analyzer. Absorption spectra were recorded on a UV-visible spectrophotometer model-UV-1650 PC (Shimadzu, Japan).

2.2. Solid State synthesis of $Yb_2V_2O_7$ nanomaterial

In a typical synthesis experiment, 0.19 g (0.5 mmol) of Yb_2O_3 (M_W = 394.08 g mol^{-1}) and 0.18 g (1 mmol) of Na_3VO_4 (M_w = 183.907 g mol^{-1}) with Yb:V molar ratio of 1:1 were mixed in a mortar until an almost homogenous powder was obtained. The obtained powder was added into a 25 mL crucible and then transferred to an electric furnace that had already reached to a desired temperature at S_1= 300°C, S_2 = 400°C, S_3 = 500°C, and S_4 = 600°C and treated thermally for 8 h. The crucible was then cooled normally in the furnace to the room temperature. The acquired powder was collected for further analyses.

2.3.Hydrothermal synthesis of $Yb_2V_2O_7$ nanomaterials

In a typical experiment for the synthesis of $Yb_2V_2O_7$, 0.19 g (0.5 mmol) of Yb_2O_3 (Mw = 394.08 g mol^{-1}) and 0.18 g (1mmol) of Na_3VO_4 (Mw = 183.907 g mol^{-1}) were added to 50 mL of hot aqueous 4M NaOH solution while stirring at 80 °C. The solution was stirred for 20 min and then transferred into a 100-mL Teflon lined stainless steel autoclave. The autoclave was sealed and heated at 180 °C for S_5 = 48 h and S_6 = 72 h. When the reaction was completed, it was cooled to the room temperature by water, immediately. The prepared powder was washed by deionized water, dried at 110 °C for 15 min under normal atmospheric condition and a white powder was collected. The obtained powder was transferred into a 25 mL crucible and treated thermally at 700 °C for 8 h. The $Yb_2V_2O_7$ synthesis yield ($M_{w=}$ 560 g mol^{-1}) was 0.19 g (70%).

3. Results and discussions

3.1. Characterization

The phase identification of the synthesized nanomaterials was performed by powder X-ray diffraction technique. Figure 1 shows the X-ray diffraction (XRD) analysis of the obtained samples in the 2θ range 10-90° as well as the structural analyses performed by the *FullProf* program. The structural analyses were performed employing profile matching with constant scale factors. Red lines are the observed intensities; the black ones are the calculated data; the blue ones are the difference: Yobs-Ycalc. The Bragg reflections positions are demonstrated by blue, red, and green bars for cubic, cubic phases of $Yb_2V_2O_7$. Figure 1 represents the PXRD patterns of the obtained $Yb_2V_2O_7$ nanomaterials. The data indicate that the PXRD patterns of the synthesized compounds at the reaction temperatures in the range of 300 to 600 °C are related to pyrochlore crystal structure and the synthesized compounds at temperature from 700 to 1000 °C are related to fluorite crystal structure. It is clear that the reaction temperature is a key factor affected the crystal phase composition. The PXRD patterns of the synthesized $Yb_2V_2O_7$ are reported in figure 1(a-f). The patterns are well fitted with the cubic crystal structure for $Yb_2V_2O_7$. The results showed that the pattern had a main $Yb_2V_2O_7$ crystal structure with space group $Fd\bar{3}m$ [11, 12, 14].

Comparing the PXRD patterns of the synthesized nanomaterials up to 600 °C shows that the obtained nanomaterials have $Yb_2V_2O_7$ crystal structure. Table 1 shows the crystallite sizes of the synthesized nanomaterials in different reaction temperatures that were calculated by Scherrer equation (equation 1). In this equation, D is the entire thickness of the crystallite sample, λ is the X-ray diffraction wavelength (0.154 nm), and k is Scherrer constant (0.9), $B_{1/2}$ of FWHM is the full width at half of its maximum intensity and θ is the half diffraction angle at which the peak is located. Also, interplanar spacing in the crystalline material was measured by Bragg's law ($n\lambda = 2d\sin(\theta)$). The data mentioned in table 1 shows that with increasing the reaction temperature, the crystallite growth was decreased from S_1 to S_4.

$$D\ (nm) = K\lambda / B_{hkl} \cos\theta \quad (1)$$

The dislocation density (δ) value is attributed to the number of defects in the crystal. The value is calculated using the crystallite size data by the below relationship:

$$\delta = \frac{1}{D^2} \quad (2)$$

The data revealed that δ value decreased confirming the improvement of the crystal nature with increasing the reaction temperature. Besides, the change in the δ value is because of the change in the crystallite size of the synthesized material through changing the reaction condition.

The strain (ε) value was calculated by the below formula:

$$\varepsilon = \frac{\beta_{hkl} \cos\theta}{4} \quad (3)$$

The variation in ε as a function of the purity of the obtained materials is included in table 1. The decrease in ε value with increase in the purity of the crystal system is probably due to the improve in the degree of crystal nature

of the obtained material. The data included in table 1 indicate that the reaction temperature affects considerably the crystallite size, strain, and dislocation density values.

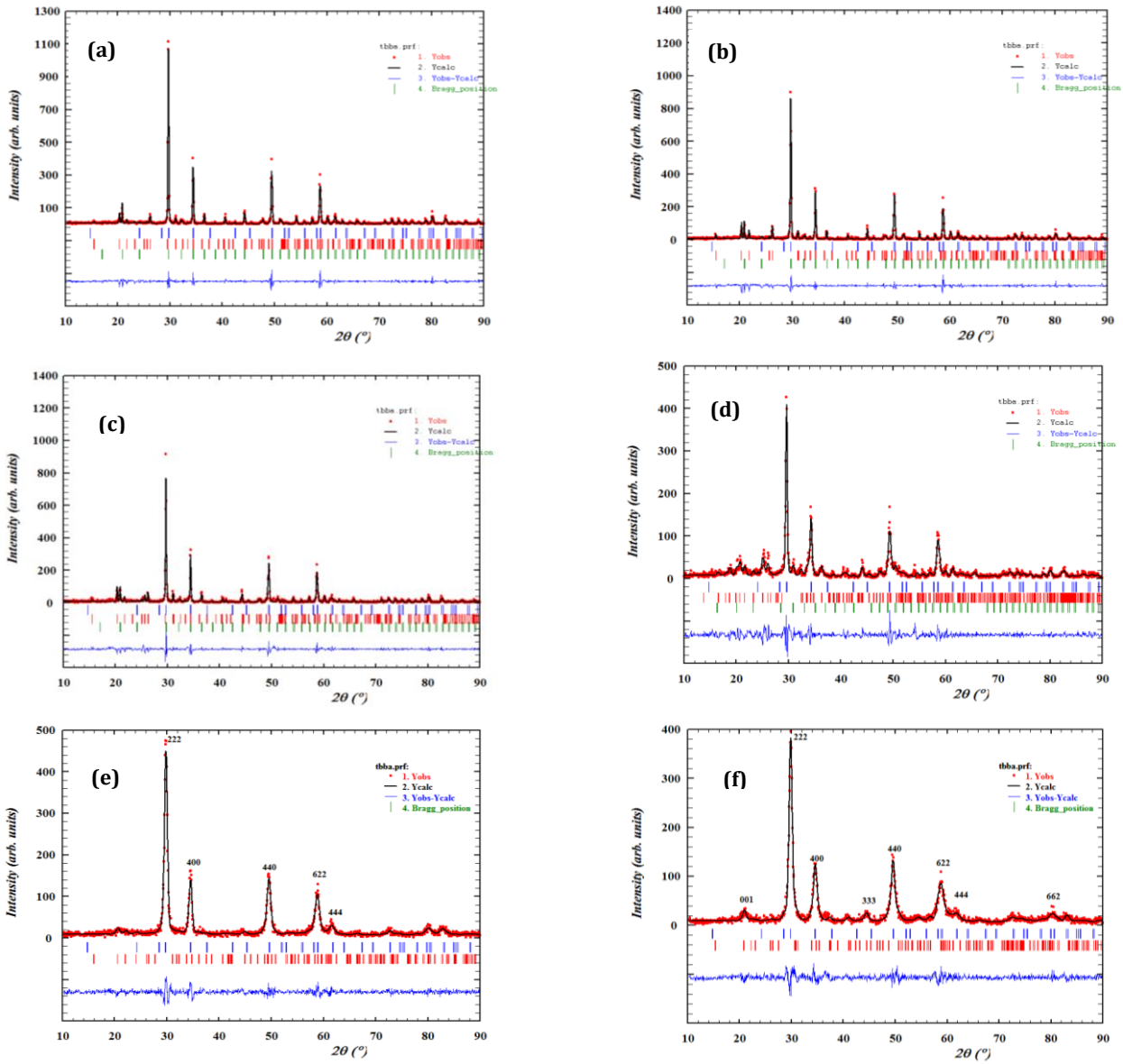

Fig. 1. X-Ray diffraction patterns and the Rietveld analyses of a) S_1, b) S_2, c) S_3, d) S_4, e) S_5, and f) S_6

Table 1. Crystallite size data for $Yb_2V_2O_7$ nanomaterials.

Data sample	2θ	$B_{1/2}$ (°)	$B_{1/2}$ (rad)	$\cos\theta_B$	Crystal size (nm)	δ	ε	Counts
S_1	29.65	0.19	0.0037	0.9667	40	0.625	0.894198	1100
S_2	29.70	0.38	0.0066	0.9665	23	0.00189	1.594725	900
S_3	29.65	0.32	0.0023	0.9667	24	0.001736	0.555853	850
S_4	29.58	0.38	0.0057	0.9668	24	0.001736	1.37769	450
S_5	29.72	0.72	0.0126	0.9665	11	0.008264	3.044475	480
S_6	29.73	0.75	0.0132	0.9665	10	0.01	3.18945	400

Table 2. Lattice parameter and interplanar spacing (d) data for the obtained Yb2V2O7 nanomaterials.

Sample	a (Å)	R_f	R_b	χ^2	Count	d(Å)	phase purity (%)
S_1	10.43	1.8	1.9	1.9	1114	3.01	85
S_2	10.43	1.9	2.6	1.9	900	3.00	84
S_3	10.43	2.3	1.7	1.9	915	3.00	82
S_4	10.45	1.1	1.5	2.1	427	3.02	80
S_5	10.41	1.4	0.5	1.5	475	2.9928	95
S_6	10.31	0.6	0.5	1.4	395	2.9859	92

of the obtained material. The data included in table 1 indicate that the reaction temperature affects considerably the crystallite size, strain, and dislocation density values.

The crystallite sizes of the obtained targets were calculated by using equation 1 and choosing a peak at about 29º for $Yb_2V_2O_7$. According to the table 1, the crystallite sizes decreased by increasing the reaction temperature.

Table 2 indicates the lattice parameters data for $Yb_2V_2O_7$ calculated by Rietveld analysis. By increasing the reaction temperature, the cell parameters values increase. R_f, R_B and χ^2 values show the goodness of the fittings. The reaction temperature is the main factor on the crystal phase growth and the purity of the obtained materials. It is clear that when the reaction temperature increases to 600 ºC, the phase purity decreases (S_1-S_4).

3.2. BET and BJH texture analysis

The synthesized powders were characterized for their surface area, average pore size and average pore volume. Prior to N_2-physical adsorption measurement, the samples were degassed at 150 °C for 120 min in the nitrogen atmosphere. So, the specific surface area (S_{BET}) of the obtained materials was determined by adsorption-desorption isotherms of N_2 at 77 K. The surface area, pore volume, and average pore diameter of the synthesized $Yb_2V_2O_7$ nanomaterials are summarized in table 3. From table 3, it can be seen that the average surface area and pore volumes are about 5.9016 m^2 g^{-1} and 0.06651 cm^3 g^{-1} for S_3, 4.2351 and 0.0612 cm^3 g^{-1} for S_4, 1.5479. m^2 g^{-1} and 0.01192 cm^3 g^{-1} for S_5, and 0.8139. m^2 g^{-1} and 0.00899 cm^3 g^{-1} for S_6, respectively. Also, the average nanoparticles sizes are 45, 57, 30, and 44 nm for S_3, S_4, S_5, and S_6, respectively. All the BET data show that the specific surface area, and pore volume of the targets are decreased with increasing the reaction temperature. Also, table 4 shows the textural properties of the as-prepared materials using BJH method. The summarized data in table 4 show that the specific surface area, pore volume, and pore sizes of S_3 are more than those of the other samples. The results of BET and BJH measurements suggest that the surface area of S_3 is larger than that of the other samples.

Table 3. BET data for $Yb_2V_2O_7$ showing the textural properties of the obtained materials.

sample	BET surface area (m^2g^{-1})	Pore volume (cm^3g^{-1})	Average particles size (nm)
S_3	5.9016	0.066514	45.082
S_4	4.2351	0.061208	57.811
S_5	1.5479	0.011928	30.824
S_6	0.81396	0.0089943	44.2

Table 4. BJH data for $Yb_2V_2O_7$ showing the textural properties of the obtained materials.

Property	S_3	S_4	S_5	S_6
BJH adsorption cumulative surface area of pores	6.3745	4.0091	1.1489	0.4484
BJH adsorption cumulative volume of pores	0.0668	0.0611	0.01176	0.0088
BJH adsorption average pore width (4V/A)	41	61	40	79

3. 3. Morphology analysis

FESEM images of the synthesized $Yb_2V_2O_7$ nanomaterials are shown in figure 2. İt is obvious in figure 2a that when the reaction temperature is 300 °C,

the morphology of this material is sponge. Figure 2b shows FESEM image of S_2. The image shows that the morphology of the obtained material is sponge. İt indicates that the diameter size of the particles that formed the sponge is in the range of 30 - 80 nm. As be can be seen from the images in figure 2c-f for the samples S3 to S6, respectively, it is clear that the materials have particle morphology with small particle sizes in the range of 30-50 nm.

3.4. Optical properties

Fig. 3 shows the optical band gap energies of the synthesized samples. According to the results of Pascual et al., the relation between the absorption coefficient and incident photon energy can be written as (αhν)2 = A(hν - Eg), where A and Eg are a constant and the direct band gap energy, respectively. Band gap energies were evaluated from extrapolating the linear part of the curve to the energy axis [26]. The band gap energies of the Yb2V2O7 nanomaterials were 2.4 eV, 3.6 eV, 4.2 eV, 4.6 eV, 2.7 eV, and 3.6 eV, respectively, for S1, S2, S3, S4, S5, and S6. The increasing of the band gap energies is attributed to the decreasing the crystallite size of the obtained materials. Besides, the XRD data showed that increasing the reaction temperature increased Yb2O3 impurity phase (Eg=4.9 eV) in the product mixture [27, 28]. So, another reason for increasing the Eg values can be increasing Yb2O3 proportion in the product mixture.

3.5. Electrochemical property

The working electrode was prepared by mixing graphite powder, silicon oil, and $Yb_2V_2O_7$ (S_1) in the ratio 10:80:10 (w/w) and the resultant mixture was homogenized using mortar. The obtained paste was tightly packed into the glass tube without any air gap. The electrical contact was made at one end by inserting a copper wire through the center of the paste packed glass tube without any crack. The exposed end of the electrode was mechanically polished and renewed using butter sheet to get reproducible smooth and shiny working surface. The electrochemical test of S_1 electrode was performed using cyclic voltammetry (CV) in a three-electrode cell containing working, reference, and counter electrodes (Figure 4).

Fig. 4 exhibits the cyclic voltammograms of $Yb_2V_2O_7$ in 1 $molL^{-1}$ NaOH and KOH aqueous solutions between -1 and +1 V at a scan rate of 10 mV s^{-1}. The CV curves of $Yb_2V_2O_7$ do not show a typical rectangular shape, confirming no pure electric double layer capacitive behavior. The substance electrochemical window (EW) is electric potential range of the electrode in which the material is not oxidized or reduced. The EW is an important characteristic that should be identified for solvents and electrolytes used in electrochemical applications. As it can be found from figure 4, it is clear that $Yb_2V_2O_7$ sample in NaOH electrolyte has a wider potential window and so $Yb_2V_2O_7$ is more stable against oxidation/reduction reaction at the same potential range compared to KOH electrolyte solution.
The following equation gives the charge discharge specific capacitance.

$$C = \frac{i \times dt}{m(Vf - Vi)} \quad (4)$$

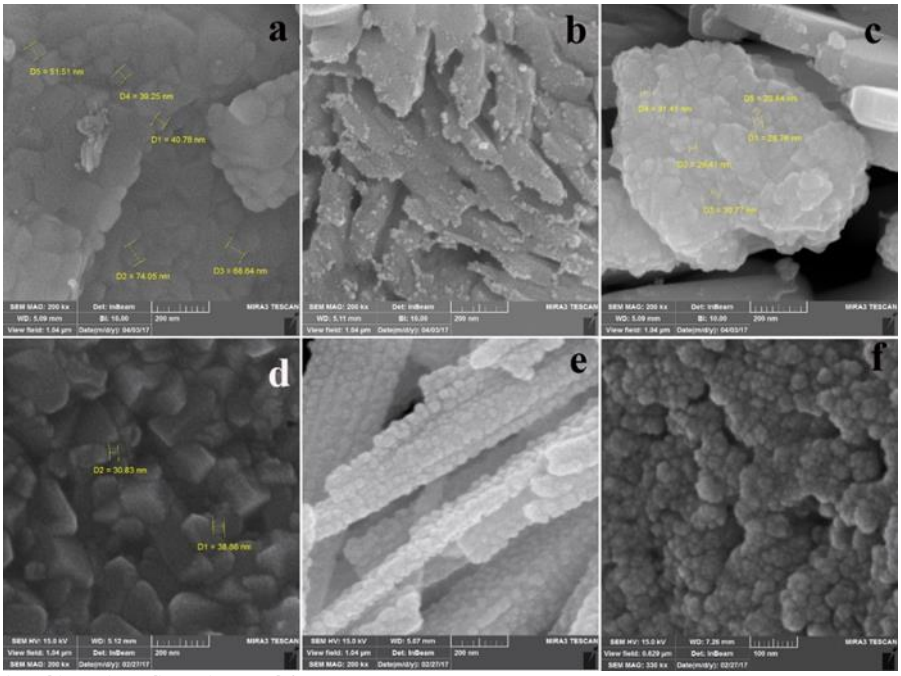

Fig. 2. FESEM images of a) S_1, b) S_2, c) S_3, d) S_4, e) S_5, and f) S_6.

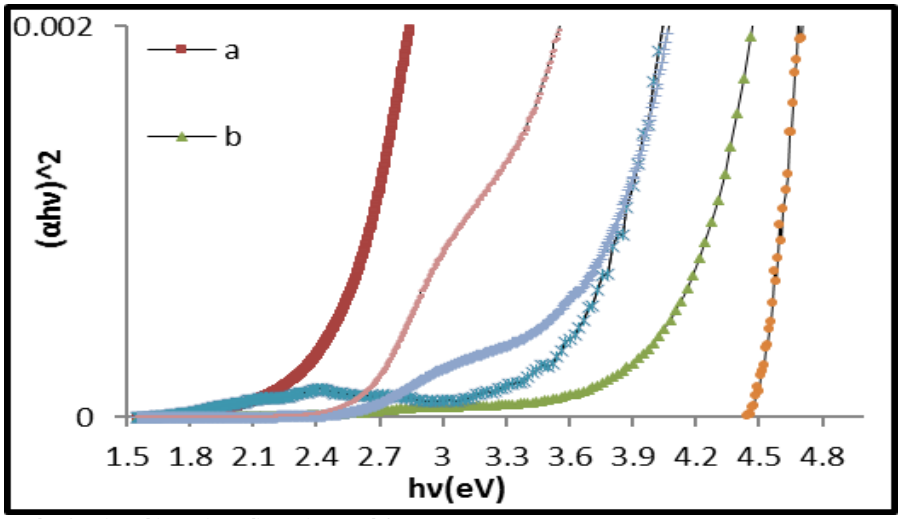

Fig. 3. Plots of $(\alpha h\nu)^2$ versus hν for a) S_1, b) S_2, c) S_3, d) S_4, e) S_5 and f) S_6.

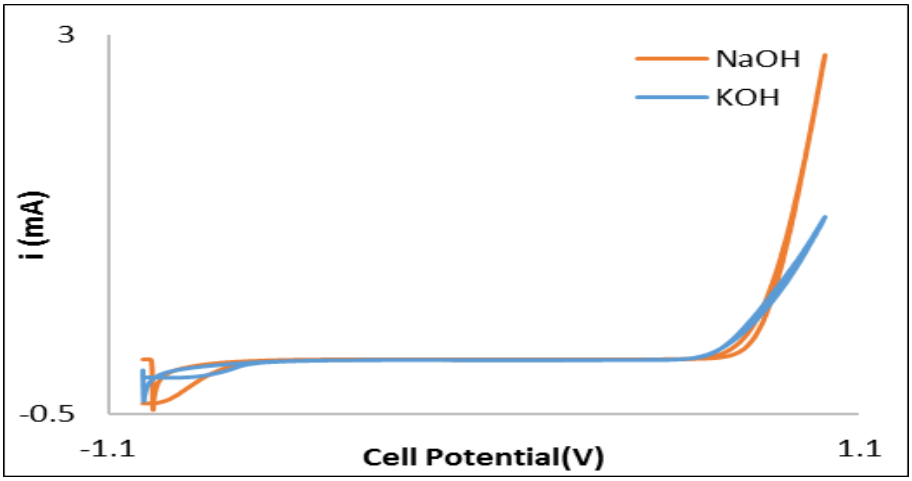

Fig. 4. CV curves of Yb2V2O7 nanoparticles measured with a scan rate of 100 mV/s.

In the equation, i is the applied current, dt is the discharging time, m is the mass of the active material coated on to the electrode, and (V_f-V_i) is the working potential window. In the present work, m is 0.01 g, i is 0.05 A/m^2, dt is 200 S. V_f-V_i is about 0.6 V. So, the C value is 1.25 A.s.g^{-1}.m^{-2}.V^{-1}.

4. Conclusion

In this work, the $Yb_2V_2O_7$ nanomaterials were synthesized successfully via solid state and hydrothermal methods. PXRD analysis corroborate the successful synthesis of the mentioned material. The Rietveld analysis showed that the reaction temperature played an important effect on the phase purity and crystal growth. FESEM image indicate that the as- synthesized nanomaterial had a mixture of rod, sponge and circle morphologies. It was found that the reaction temperature and time has a main effect on the morphology of the nanomaterials obtained. UV-Vis spectra of the synthesized nanomaterial were investigated and band gap energies were calculated. CV analysis data confirmed the electrochemical activity of $Yb_2V_2O_7$ nanomaterial.

Conflict of interest

The authors declare they have no conflict of interest for the present work.

References

[1] A.R. Cleave, "Atomic scale simulations for waste form applications." in University of London London, UK, (2006).

[2] J.B. Thomson, A.R. Armstrong, P.G. Bruce, "An oxygen-rich pyrochlore with fluorite composition." Journal of Solid State Chemistry 148 (1999) 56-62.

[3] H. Kishimoto, T. Omata, S. Otsuka-Yao-Matsuo, K. Ueda, H. Hosono, H. Kawazoe, "Crystal structure of metastable κ-CeZrO4 phase possessing an ordered arrangement of Ce and Zr ions." Journal of alloys and compounds 312 (2000) 94-103.

[4] D.J. Haynes, D.A. Berry, D. Shekhawat, J.J. Spivey, "Catalytic partial oxidation of n-tetradecane using pyrochlores: Effect of Rh and Sr substitution." Catalysis Today 136 (2008) 206-213.

[5] R. Kieffer, M. Fujiwara, L. Udron, Y. Souma, "Hydrogenation of CO and CO_2 toward methanol, alcohols and hydrocarbons on promoted copper-rare earth oxides catalysts." Catalysis today 36 (1997) 15-24.

[6] K. Matsuhira, M. Wakeshima, Y. Hinatsu, S. Takagi, "Metal–Insulator Transitions in Pyrochlore Oxides Ln 2Ir2O7." Journal of the Physical Society of Japan 80 (2011) 094701.

[7] K. Ross, L. Yaraskavitch, M. Laver, J.S. Gardner, J. Quilliam, S. Meng, J. Kycia, D. Singh, T. Proffen, H. Dabkowska, "Dimensional evolution of spin correlations in the magnetic pyrochlore $Yb_2Ti_2O_7$." Physical Review B 84 (2011) 174442.

[8] S. Khademinia, M. Behzad, "Lanthanum cerate ($La_2Ce_2O_7$): hydrothermal synthesis, characterization and optical properties." International Nano Letters 5 (2015) 101-107.

[9] C. Shen, X. Tang, S.A. Cheema, C. Zhang, M.I. Khan, F. Liang, X. Chen, Y. Zhu, Q. Lin, Y. Chen, "Enhanced phytoremediation potential of polychlorinated biphenyl contaminated soil from e-waste recycling area in the presence of randomly methylated-β-cyclodextrins." Journal of hazardous materials 172 (2009) 1671-1676.

[10] J.K. Gill, O. Pandey, K. Singh, "Ionic conductivity, structural and thermal properties of pure and Sr^{2+} doped Y2Ti2O7 pyrochlores for SOFC." Solid State Sciences 13 (2011) 1960-1966.

[11] T. Shin-Ike, G. Adachi, J. Shiokawa, "On the pyrochlore type $Ln_2V_2O_7$ (Ln: Rare-earth elements)." Materials Research Bulletin 12 (1977) 1149-1154.

[12] Z. Dun, J. Ma, H. Cao, Y. Qiu, J. Copley, T. Hong, M. Matsuda, J. Cheng, M. Lee, E. Choi, "Competition between the inter-and intra-sublattice interactions in $Yb_2V_2O_7$." Physical Review B 91 (2015) 064425.

[13] L. Soderholm, C. Stager, J. Greedan, "Crystal field effects on the magnetic behavior of $Yb_2V_2O_7$ and Tm2V2O7." Journal of Solid State Chemistry 43 (1982) 175-180.

[14] L. Soderholm, J. Greedan, M. Collins, "Bulk magnetic and neutron diffraction data for the pyrochlore $Yb_2V_2O_7$: Evidence for ferromagnetic coupling between Yb3+ and V4+ moments." Journal of Solid State Chemistry 35 (1980) 385-390.

[15] A. Kaminskii, S. Bagayev, K. Oka, H. Shibata, K. Ueda, K. Takaichi, H. Eichler, H. Rhee, "Observation of stimulated Raman scattering in the tetragonal crystal $YbVO_4$, Laser." Physics Letters 3 (2006) 263.

[16] A. Kaminskii, H. Eichler, H. Rhee, K. Ueda, K. Oka, H. Shibata, "New nonlinear-laser effects in $YbVO_4$ crystal: Sesqui-octave stokes and anti-Stokes comb generation and the cascaded self-frequency "tripling" of χ (3)-Stokes components under a one-micron picosecond pumping." Laser physics 18 (2008) 1546-1552.

[17] V. Panchal, D. Errandonea, A. Segura, P. Rodriguez-Hernandez, A. Muñoz, S. Lopez-Moreno, M. Bettinelli, "The electronic structure of zircon-type orthovanadates: Effects of high-pressure and cation substitution." Journal of Applied Physics 110 (2011) 043723.

[18] W. Hutchison, M. Prandolini, D. Chaplin, G. Bowden, B. Bleaney, "A nuclear orientation study of $YbVO_4$." Czechoslovak Journal of Physics 46 (1996) 2151-2152.

[19] C. Santos, I. Guedes, C.-K. Loong, L.A. Boatner, "Low-temperature Raman spectra of $YbVO_4$." Vibrational Spectroscopy 45 (2007) 95-98.

[20] Z. Xu, Q. Zhao, T. Liu, L. Wang, S. Bian, "Uniform and Well-Dispersed $YbVO_4$ Hierarchical Nanoarchitectures: Synthesis and Luminescence Properties." Journal of nanoscience and nanotechnology 13 (2013) 344-350.

[21] P.C. de Sousa Filho, T. Gacoin, J.P. Boilot, R.I. Walton, O.A. Serra, "Synthesis and luminescent properties of $REVO_4$–$REPO_4$ (RE= Y, Eu, Gd, Er, Tm, or Yb) heteronanostructures: a promising class of phosphors for excitation from NIR to VUV." The Journal of Physical Chemistry C 119 (2015) 24062-24074.

[22] Y. Cheng, H. Zhang, K. Zhang, Z. Xin, X. Yang, X. Xu, W. Gao, D. Li, C. Zhao, J. Xu, "Growth and spectroscopic characteristics of Er^{3+}: $YbVO_4$ crystal." Journal of Crystal Growth 311 (2009) 3963-3968.

[23] B.C. Chakoumakos, M.M. Abraham, L.A. Boatner, "Crystal structure refinements of zircon-type MVO_4 (M= Sc, Y, Ce, Pr, Nd, Tb, Ho, Er, Tm, Yb, Lu)." Journal of Solid State Chemistry 109 (1994) 197-202.

[24] M. Goudarzi, A. Abedini, "Synthesis, characterization, and investigation of magnetic and photocatalytic property of $YbVO_4$ nanoparticles." Journal of Materials Science: Materials in Electronics 28 (2017) 114-119.

[25] Z. Huang, L. Zhang, W. Pan, Synthesis, "lattice dynamics, and mechanical properties of a high-pressure scheelite phase of RVO_4." Inorganic chemistry 51 (2012) 11235-11237.

[26] M. Goudarzi, A. Abedini, "Synthesis, characterization, and investigation of magnetic and photocatalytic property of $YbVO_4$ nanoparticles." Journal of Materials Science: Materials in Electronics 28 (2017) 114-119.

[27] J. Pascual, J. Camassel, H. Mathieu, "Fine structure in the intrinsic absorption edge of TiO_2." Physical Review B 18 (1978) 5606.

[28] S. Ohmi, C. Kobayashi, I. Kashiwagi, C. Ohshima, H. Ishiwara, and H. Iwai, "Characterization of La_2O_3 and Yb_2O_3 Thin Films for High-k Gate Insulator Application." Journal of The Electrochemical Society 150 (2003) 140.